EPJ manuscript No.
(will be inserted by the editor)

Trace of $\Lambda(1405)$ resonance in low energy $K^- + {}^3\mathrm{He} \to (\pi^0\Sigma^0) + d$ reaction

J. Esmaili[1], S. Marri[2], M. Raeisi[1] and A. Naderi Beni[3]

[1] Department of Physics, Faculty of Basic Sciences, Shahrekord University, Shahrekord, 115, Iran
[2] Department of Physics, Isfahan University of Technology, Isfahan 84156-83111, Iran
[3] Department of Physics, Payame Noor University, P. O. Box 19395-3697, Tehran, Iran

Received: date / Revised version: date

Abstract. In present work, we investigated $K^- + {}^3\mathrm{He}$ reaction at low energies. The coupled-channel Faddeev AGS equations were solved for $\bar{K}Nd - \pi\Sigma d$ three-body system in momentum representation to extract the scattering amplitudes. To trace the signature of the $\Lambda(1405)$ resonance in the $\pi\Sigma$ invariant mass, the deuteron energy spectrum for $K^- + {}^3\mathrm{He} \to \pi\Sigma d$ reaction was obtained. Different types of $\bar{K}N - \pi\Sigma$ potentials based on phenomenological and chiral SU(3) approaches were used. As a remarkable result of this investigation, it was found that the deuteron energy spectrum, reflecting the $\Lambda(1405)$ mass distribution and width, depends quite sensitively on the $\bar{K}N - \pi\Sigma$ model of interaction. Hence accurate measurements of the $\pi\Sigma$ mass distribution have the potential to discriminate between possible mechanisms at work in the formation of the $\Lambda(1405)$.

PACS. 13.75.Jz, 14.20.Pt, 21.85.+d, 25.80.Nv describing text of that key

1 Introduction

An important issue in various aspects in strangeness nuclear physics is the structure of $\Lambda(1405)$ resonance, which has been found to be a highly controversies topic in studying the antikaon-nucleon interaction. The $\Lambda(1405)$ resonance is a bound state of $\bar{K}N$, which exclusively decays into the $\pi\Sigma(I = 0)$ channel via the strong interaction. The $\bar{K}N - \pi\Sigma$ interaction, which is a fundamental ingredient of the antikaonic nuclear clusters [1, 2, 3, 4, 5, 6, 7, 8, 9, 10, 11, 12, 13, 14, 15, 16] is also strongly dominated by $\Lambda(1405)$ resonance. The existence of $\Lambda(1405)$ resonance was first predicted by Dalitz and Tuan [17, 18] in 1959 showing that the unitarity in coupled-channel $\bar{K}N - \pi\Sigma$ system leads to the existence of $\Lambda(1405)$. As early as in 1961 an experimental evidence of this resonance was reported in the invariant mass spectrum of the $\pi\Sigma$ resulting from $K^- p \to \pi\pi\pi\Sigma$ reaction [19] at 1.15 GeV.

The $\bar{K}N$ interaction models which reproduce the mass of $\Lambda(1405)$ resonance and two-body scattering data can be divided into two classes: those constructed phenomenologically [5, 6, 20] and those derived based on chiral SU(3) dynamics [7, 8, 9, 10, 11]. Even though the phenomenological and the chiral SU(3) $\bar{K}N$ interaction models produce comparable results at and above $\bar{K}N$ threshold, they differ significantly in their extrapolations to sub-threshold energies [21]. The phenomenological $\bar{K}N$ potentials are constructed to describe the $\Lambda(1405)$ as a single pole of the scattering amplitude around 1405 MeV, corresponding to a quasi-bound state of the $\bar{K}N$ system with a binding energy of about 30 MeV. On the other hand, the $\bar{K}N - \pi\Sigma$ coupled-channels amplitude resulting from chiral SU(3) dynamics has two poles. The two poles are commonly characterized as following: the first pole in the complex energy plane is located quite close to the $\bar{K}N$ threshold with a small imaginary part, around 10-30 MeV, and a strong coupling to $\bar{K}N$. In turn, the second one is wider, with a relatively large imaginary part around 50-200 MeV, coupling more strongly to the $\pi\Sigma$ channel and its pole position shows more dependence on the specific theoretical model [22, 23, 24, 25, 26, 27]. This different pole structure comes from different off-shell properties of the $\bar{K}N$ interactions. The $\bar{K}N$ interactions based on the chiral SU(3) dynamics are energy-dependent, and that in the sub-threshold become less attractive than those proposed by the energy-independent phenomenological potentials [21].

The $\pi\Sigma$ mass spectrum is a suitable tools to study the $\bar{K}N$ reaction below the $\bar{K}N$ threshold. As it is impossible to perform the scattering experiment in the $\pi\Sigma$ channel directly, the resonance properties can be extracted by analyzing the invariant mass distribution of the $\pi\Sigma$ final state in reactions that produce $\Lambda(1405)$ resonance. During the past decades, many experimental and theoretical searches were carried out to investigate the possible observation of $\Lambda(1405)$ resonance. Braun *et al.,* studied the $K^- d$ reaction and reported a resonance energy around 1420 MeV [28]. In Ref. [29], the pion induced reaction $(\pi^- p \to K^+\pi\Sigma)$ was investigated and the mass of the resonance was found to be consistent with 1405 MeV. Using photoproduction reactions, the CLAS [30, 31, 32] and LEPS [33, 34] collaboration investigated the $\Lambda(1405)$ resonance signal. Several theoretical studies have been done to analyze the CLAS data using different interaction models for $\bar{K}N$ system, which are based on chiral SU(3) dynamics [35, 36, 37, 38, 39] and phenomenological approachs [40]. Other interesting experiments were also performed at GSI by HADES collaboration [41] and

at J-PARC as an E31 experiment [42] to clarify the nature of the $\Lambda(1405)$ by using pp and K^-d reactions, respectively. In the E31 experiment, the $\pi\Sigma$ mass spectra are measured for all combinations of charges, i.e., $\pi^\pm\Sigma^\mp$ and $\pi^0\Sigma^0$. To establish a theoretical framework for a detailed analysis of K^-d reaction, different theoretical studies were performed. The theoretical investigations of $K^-d \to \pi\Sigma + n$ have been performed in [43, 44, 45, 46] using a two-step process. The differential cross sections of K^-d reaction were also studied in Refs. [47, 48] using three-body Faddeev method and it was demonstrated that the K^-d reaction can be a useful tool for studying the subthreshold properties of the $\bar{K}N$ interaction.

The $K^- + {}^3\mathrm{He}$ reaction was studied in Ref. [49] using variational method. The $\Sigma\pi$ invariant-mass spectrum in the resonant capture of K^- at rest in ${}^3\mathrm{He}$ were calculated by a coupled-channel potential for $\bar{K}N - \pi\Sigma$ interaction. The results in Ref. [49] confirmed the $\Lambda(1405)$ ansatz and the proposed predictions by chiral-SU(3) ($M \sim 1420$ MeV/c^2) were excluded. The authors finally proposed more stringent test by using a ${}^3\mathrm{He}$ target. An experimental search for $\bar{K}NN$ bound state was performed at J-PARC by using the in-flight $K^- + {}^3\mathrm{He}$ reaction at 1 GeV/c [50]. In the E15 experiment, the $\pi\Sigma$ invariant mass spectrum resulting from $K^- + {}^3\mathrm{He}$ reaction was measured for two combinations of charges, i.e., $\pi^\pm\Sigma^\mp pn$. It was shown that the production cross section of the $\Lambda(1405)p$ is ~ 10 times larger than that of the K^-pp bound state observed in Λp invariant mass which is an important information on the production mechanism of the K^-pp bound state [50].

The purpose of the present work is to explore the $\pi\Sigma$ invariant mass spectra resulting from the $K^- + {}^3\mathrm{He} \to \pi\Sigma d$ reaction. The problem can be solved using methods developed within three-body theories. To reduce the four-body $K^- + {}^3\mathrm{He}$ system to a three-body system, we considered a $p - d$ cluster structure for ${}^3\mathrm{He}$ nuclei (Fig. 1). To study this reaction, the Faddeev amplitudes for $\bar{K}Nd - \pi\Sigma d$ system were calculated at real scattering energies. One of the aims is to study the role of different off-shell properties of the underlying interactions as they are realized in chiral SU(3) dynamics versus phenomenological potential models. With this method, we investigated how well the $\Lambda(1405)$ resonance manifests itself in the three-body observable. To study the dependence of the $K^- + {}^3\mathrm{He}$ reaction on the fundamental $\bar{K}N - \pi\Sigma$ interaction, different interaction models derived from chiral SU(3) and phenomenological approaches, were included in our calculations.

The paper is organized as follows: in Sect. 2, we will explain the Faddeev formalism used for the three-body $\bar{K}Nd$ system and give a brief description of scattering amplitude for $K^- + {}^3\mathrm{He} \to \pi\Sigma d$ reaction. The two-body inputs of the calculations and the extracted results for $\pi\Sigma$ mass spectra are presented in Sect. 3 and in Section 4, we give conclusions.

2 Three-body treatment of $K^- + {}^3\mathrm{He}$ reaction

In the present work, the possible signature of the $\Lambda(1405)$ resonance in $\pi\Sigma$ mass spectrum resulting from $K^- + {}^3\mathrm{He} \to \pi\Sigma d$ reaction was studied. We used the three-body Faddeev AGS equations [51]. As there are three different particles in the system under consideration, we will have the following partitions of the $\bar{K}Nd$ three-body system, defining the interacting pairs and their allowed spin and isospin quantum numbers

$$\begin{aligned}(1) &: \bar{K} + (Nd)_{s=\frac{1}{2};I=\frac{1}{2}},\\ (2) &: N + (\bar{K}d)_{s=1;I=\frac{1}{2}},\\ (3) &: d + (\bar{K}N)_{s=\frac{1}{2};I=0}.\end{aligned} \tag{1}$$

The quantum numbers of the $\bar{K}Nd$ are $I = 0$ and $s = \frac{1}{2}$, in actual calculations, when we include isospin and spin indices the number of configurations is equal to three, corresponding to different possible two-quasi-particle partitions.

The key point of the present calculations is the separable representation of the scattering amplitudes in the two-body subsystems. The separable potentials for two-body subsystems are given by

$$V_i^{I_i}(k,k') = g_i^{I_i}(k)\,\lambda_i^{I_i}\,g_i^{I_i}(k'), \tag{2}$$

where $g_i^{I_i}(k)$ is used to define the form factor of the interacting two-body subsystem with relative momentum k and isospin I and $\lambda_i^{I_i}$ defines the strength of the interaction. The two-body interactions are also labeled by the i values to define simultaneously the spectator particle and interacting pair. Using separable potentials, we can define the two-body t-matrices in the following form

$$T_i^{I_i}(k,k';z) = g_i^{I_i}(k)\,\tau_i^{I_i}(z - \frac{p_i^2}{2\eta_i})\,g_i^{I_i}(k'), \tag{3}$$

where the $\tau_i^{I_i}(z)$-functions are the two-body propagators embedded in three-body system and p_i is the spectator particle momentum. The reduced mass η_i is also given by

$$\eta_i = m_i(m_j + m_k)/(m_i + m_j + m_k). \tag{4}$$

The whole dynamics of $\bar{K}Nd$ three-body system is described in terms of the transition amplitudes $\mathcal{K}^{I_iI_j}_{i,m;j,n}$, which connect the quasi-two-body channels characterized by Eq. 1. In Fig. 2, the three different rearrangement channels of the $\bar{K}Nd$ are represented. The Faddeev AGS equations for $\bar{K}Nd$ systems can be expressed by

$$\begin{aligned}\mathcal{K}^{I_{\bar{K}}I_{\bar{K}}}_{\bar{K},m;\bar{K},n} &= \sum_{rr'}\mathcal{M}^{I_{\bar{K}}I_N}_{\bar{K},m;N,r}\tau^{I_N}_{N(rr')}\mathcal{K}^{I_NI_{\bar{K}}}_{N,r';\bar{K},n}\\ &\quad+\sum_{rr'}\mathcal{M}^{I_{\bar{K}}I_d}_{\bar{K},m;d,r}\tau^{I_d}_{d(rr')}\mathcal{K}^{I_dI_{\bar{K}}}_{d,r';\bar{K},n}\\ \mathcal{K}^{I_NI_{\bar{K}}}_{N,m;\bar{K},n} &= \mathcal{M}^{I_NI_{\bar{K}}}_{N,m;\bar{K},n} + \sum_{rr'}\mathcal{M}^{I_NI_{\bar{K}}}_{N,m;\bar{K},r}\tau^{I_{\bar{K}}}_{\bar{K}(rr')}\mathcal{K}^{I_{\bar{K}}I_{\bar{K}}}_{\bar{K},r';\bar{K},n}\\ &\quad+\sum_{rr'}\mathcal{M}^{I_NI_d}_{N,m;d,r}\tau^{I_d}_{d(rr')}\mathcal{K}^{I_dI_{\bar{K}}}_{d,r';\bar{K},n}\\ \mathcal{K}^{I_dI_{\bar{K}}}_{d,m;\bar{K},n} &= \mathcal{M}^{I_dI_{\bar{K}}}_{d,m;\bar{K},n} + \sum_{rr'}\mathcal{M}^{I_dI_{\bar{K}}}_{d,m;\bar{K},r}\tau^{I_{\bar{K}}}_{\bar{K}(rr')}\mathcal{K}^{I_{\bar{K}}I_{\bar{K}}}_{\bar{K},r';\bar{K},n}\\ &\quad+\sum_{rr'}\mathcal{M}^{I_dI_N}_{d,m;N,r}\tau^{I_N}_{N(rr')}\mathcal{K}^{I_NI_{\bar{K}}}_{N,r';\bar{K},n}.\end{aligned} \tag{5}$$

Here, the operators $\mathcal{K}^{I_iI_j}_{i,m;j,n}$ are the three-body transition amplitudes, which describe the dynamics of the three-body $\bar{K}Nd$

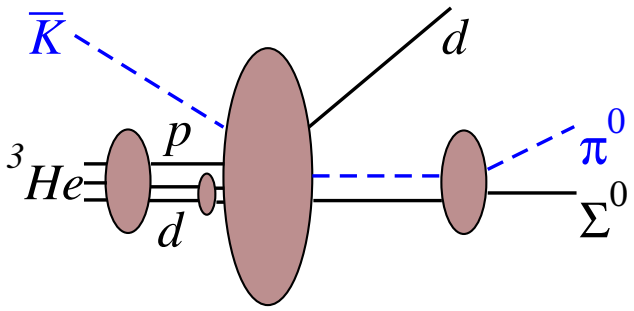

Fig. 1. (Color on line) Diagrammatic representation for $K^- + {}^3\mathrm{He} \to (\pi\Sigma) + d$ reaction using a $p-d$ cluster structure for ${}^3\mathrm{He}$ nuclei.

system. To define the spectator particles or interacting particles in each subsystem, we used the i, j and k indices and the isospin of the interacting particles is defined by I_i. Since some potentials are rank-2, the indices n, l, m are used to define, which term of the sub-amplitudes is used. The operators $\mathcal{M}^{I_iI_j}_{i,m;j,n}$ are Born terms, which describe the effective particle-exchange potential realized by the exchanged particle between the quasi-particles in channels i and j. The Born terms are defined by

$$\mathcal{M}^{I_iI_j}_{i,m;j,n}(p_i,p_j;z) = \frac{\Omega_{I_iI_j}}{2} \times \int_{-1}^{+1} dx \, \frac{g^{I_i}_{i,m}(q_i)\, g^{I_j}_{j,n}(q_j)}{z - \frac{p_i^2}{2m_i} - \frac{p_j^2}{2m_j} - \frac{(\boldsymbol{p}_i+\boldsymbol{p}_j)^2}{2m_k}}, \tag{6}$$

where the parameters $\Omega_{I_iI_j}$ are the spin and isospin coupling coefficients. The momenta $\boldsymbol{q}_i(\boldsymbol{p}_i,\boldsymbol{p}_j)$ and $\boldsymbol{q}_j(\boldsymbol{p}_i,\boldsymbol{p}_j)$ are given in terms of $\boldsymbol{p}_i$ and $\boldsymbol{p}_j$. We use the relations

$$\begin{aligned} \boldsymbol{q}_i &= -\boldsymbol{p}_j - \frac{m_j}{m_j+m_k}\boldsymbol{p}_i, \\ \boldsymbol{q}_j &= \boldsymbol{p}_i + \frac{m_i}{m_i+m_k}\boldsymbol{p}_j, \end{aligned} \tag{7}$$

where m_k is exchanged particle or quasi-particle mass and x is defined by $x = \hat{p}_i \cdot \hat{p}_j$.

For the $K^- + {}^3\mathrm{He}$ reaction, the initial state in the laboratory frame contains an incoming kaon, the projectile, and one ${}^3\mathrm{He}$, the target, at rest. There are three possibilities for the final state. In one, the ${}^3\mathrm{He}$ survives scattering, i.e. the final state contains a kaon and a ${}^3\mathrm{He}$. This is called elastic scattering. The other is where the system goes to $(\bar{K}N) + d$ and $(\bar{K}d) + N$ channel.

3 Results and discussion

Before we proceed to discus about the obtained results, we shall begin with a survey on the two-body interactions, which are the central input to our present three-body calculations. For all two-body interactions, the angular momentum is taken to be zero and all potentials have the separable form in momentum representation.

Different phenomenological and chiral based potentials were used to describe the $\bar{K}N - \pi\Sigma$ interaction, which is the most important input in the $\bar{K}Nd - \pi\Sigma d$ three-body system. The phenomenological potentials SIDD^1 and SIDD^2 from Ref. [53] are constructed to reproduce the SIDDHARTA [54] experiment results. SIDD^1 and SIDD^2 potentials reproduce the one- and two-pole structure of $\Lambda(1405)$, respectively. The potentials have the following form

$$V^I_{\alpha\beta}(k,k') = g^I_\alpha(k)\, \lambda^I_{\alpha\beta}\, g^I_\beta(k'). \tag{8}$$

Here, the strength parameters and the form factors of the two-body potential are labeled by particle indices α and β to take into account the coupling between $\bar{K}N$ and $\pi\Sigma$ systems. To study the dependence of the results to the $\bar{K}N - \pi\Sigma$ model of interaction, we also used the potential given by Akaishi and Yamazaki [1] and the new potential given in Ref. [55] which the first one is an extremely deep potential. We referred to these potentials as AY and Rev-A potentials, respectively. The Rev-A model is a chiral based but energy-independent potential which is a rather new and probably not well known. Five different interaction models (A-E) are presented in Ref. [55]. As the A model reproduce the lowest value of χ, the A version was chosen to be used in present calculations. Most of chiral potentials in the literatures are not suitable for Faddeev calculation or at least will make the calculations difficult. The last $\bar{K}N$ potential that we used in our calculations is an energy-dependent chiral potential (Chiral-IKS). The parameters of the energy-dependent chiral based potential are presented in Ref. [11]. In Table 1, the pole position(s) of the $\bar{K}N$ system for all models of interaction are presented.

Two models of interaction were used to describe the pd interaction. The first one is a two terms potential, which includes the short range repulsive part of the interaction

$$V^{Nd}_A(k,k') = \sum_{m=1}^{2} g^{Nd}_{A;m}(k)\, \lambda^{Nd}_{A;m}\, g^{Nd}_{A;m}(k'), \tag{9}$$

where the functions $g^{Nd}_i(k)$ are the form factors of pd interaction and are parametrized by Yamaguchi form [56]:

$$g^{Nd}_{A;m}(k) = \frac{1}{k^2 + (\Lambda^{Nd}_{A;m})^2}. \tag{10}$$

We refer to the two-term potential as V^{Nd}_A. The parameters of the V^{Nd}_A potential are adjusted to reproduce the $p-d$ phase-shifts [57]. The physical values for data fitting were obtained

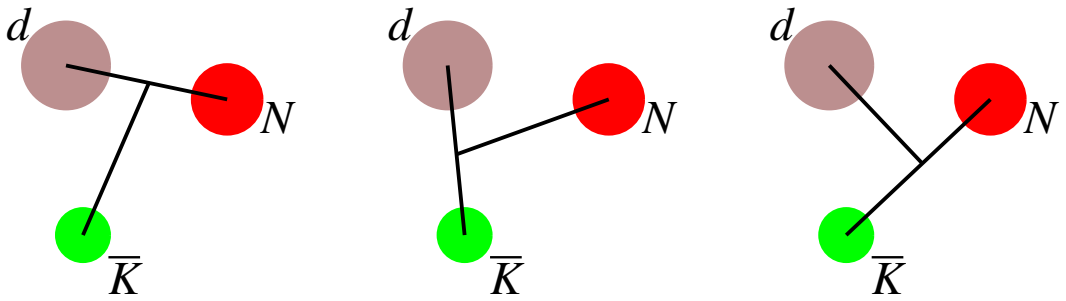

Fig. 2. (Color on line) Diagrammatic representation for different partitions of the $\bar{K}Nd$ system. Defining the interacting particles, we will have three partitions, namely $\bar{K} + (Nd)$, $(\bar{K}d) + N$ and $(\bar{K}N) + d$. The anti-kaon is defined by green circle, the nucleon by red circle and the deuteron by brown circle.

Table 1. The pole position(s) (in MeV) of the $\bar{K}N$ system for different phenomenological and chiral based models of the $\bar{K}N - \pi\Sigma$ interaction. X^1 and X^2 stands for a one- and a two-pole version of the SIDD potentials. The quantities p_1 and p_2 represent the first and second pole of $\bar{K}N - \pi\Sigma$ system for each potential.

	SIDD^1	SIDD^2	$\mathrm{Chiral-IKS}$	AY	$\mathrm{Rev}-A$
p_1	$1428.1 - i46.6$	$1418.1 - i56.9$	$1420.6 - i20.3$	$1407.6 - i20.0$	$1422.0 - i20.0$
p_2	–	$1382.0 - i104.2$	$1343.0 - i72.5$	–	–

by solving the Lippmann-Schwinger equations without inclusion of the Coulomb interaction into the $p-d$ system. We used also a one-term potential for pd interaction and its parameter are adjusted to reproduce the ${}^3\mathrm{He}$ binding energy and pd scattering length. We refer to the rank one potential as V_B^{Nd}. The parameters of the the V_A^{Nd} and V_B^{Nd} potentials are presented in Table 2

Table 2. The parameters of V_A^{Nd} and V_B^{Nd} potentials to describe the pd interaction. The range parameters are in MeV and the strength parameters are in fm^{-2}.

V_A^{Nd} potential:				
	$\Lambda_{A;1}^{Nd}$	$\Lambda_{A;2}^{Nd}$	$\lambda_{A;1}^{Nd}$	$\lambda_{A;2}^{Nd}$
	115	152	-0.0404	0.2967
V_B^{Nd} potential:				
	Λ_B^{Nd}	λ_B^{Nd}		
	139.1	-0.0037		

We need also a potential model to describe the interaction between antikaon and deuteron. A one-channel complex potential with rank-2 were used to describe K^-d interaction

$$V^{\bar{K}d}(k,k') = \sum_{m=1}^{2} g_m^{\bar{K}d}(k)\, \lambda_{m;Complex}^{\bar{K}d}\, g_m^{\bar{K}d}(k'). \qquad (11)$$

The parameters of this potential are given in Ref. [58]. The complex strength parameters and range parameters of the potential are adjusted to reproduce the K^-d scattering length a_{K^-d} and also the effective range $r^0_{K^-d}$ [58].

3.1 The one-channel AGS calculation of the $\bar{K}Nd - \pi\Sigma d$

To take the coupling between $\bar{K}N$ and $\pi\Sigma$ channels into account, the formalism of Faddeev equations should be extended to include the $\pi\Sigma d$ channel. In the present subsection, the $\pi\Sigma d$ channel of the $\bar{K}Nd$ system has not been included directly and one-channel Faddeev AGS equations are solved for three-body $\bar{K}Nd$ system and we approximated the full coupled-channel interaction by using the so-called exact optical $\bar{K}N(-\pi\Sigma)$ potential [52]. Therefore, the decaying to the $\pi\Sigma d$ channel is taken into account through the imaginary part of the optical $\bar{K}N(-\pi\Sigma)$ potential. To study the possible signature of the $\Lambda(1405)$ resonance in the $\pi^0\Sigma^0$ mass spectra in the $K^- + (Nd) \to \pi\Sigma + d$ reaction, first we should define break-up amplitude. As we do not include the lower lying channels directly into the calculations, the only Faddeev amplitude, which contribute in the scattering amplitude is $\mathcal{K}_{d,\bar{K}}$. Therefore, the break-up amplitude can be expressed as

$$T_{(\pi\Sigma)+d\leftarrow\bar{K}+(Nd)}(\boldsymbol{k}_d, \boldsymbol{p}_d, \bar{p}_{\bar{K}}; z) = \sum_{n=1}^{2} g_{\pi\Sigma}^{I=0}(\boldsymbol{k}_d) \times \tau_{(\pi\Sigma)\leftarrow(\bar{K}N)}^{I=0}(z - \frac{p_d^2}{2\eta_d})\mathcal{K}_{d,1;\bar{K},n}^{0\,\frac{1}{2}}(p_d, \bar{p}_{\bar{K}}; z), \qquad (12)$$

where $\boldsymbol{k}_i$ is the relative momentum between the interacting pair (jk) and $\bar{p}_{\bar{K}}$ is the initial momentum of $\bar{K}$ in $\bar{K}Nd$ center of mass. The quantity $\mathcal{K}_{i(m),j(n)}^{I_iI_j}$ is the Faddeev amplitude, which is derived from Faddeev equation (5).

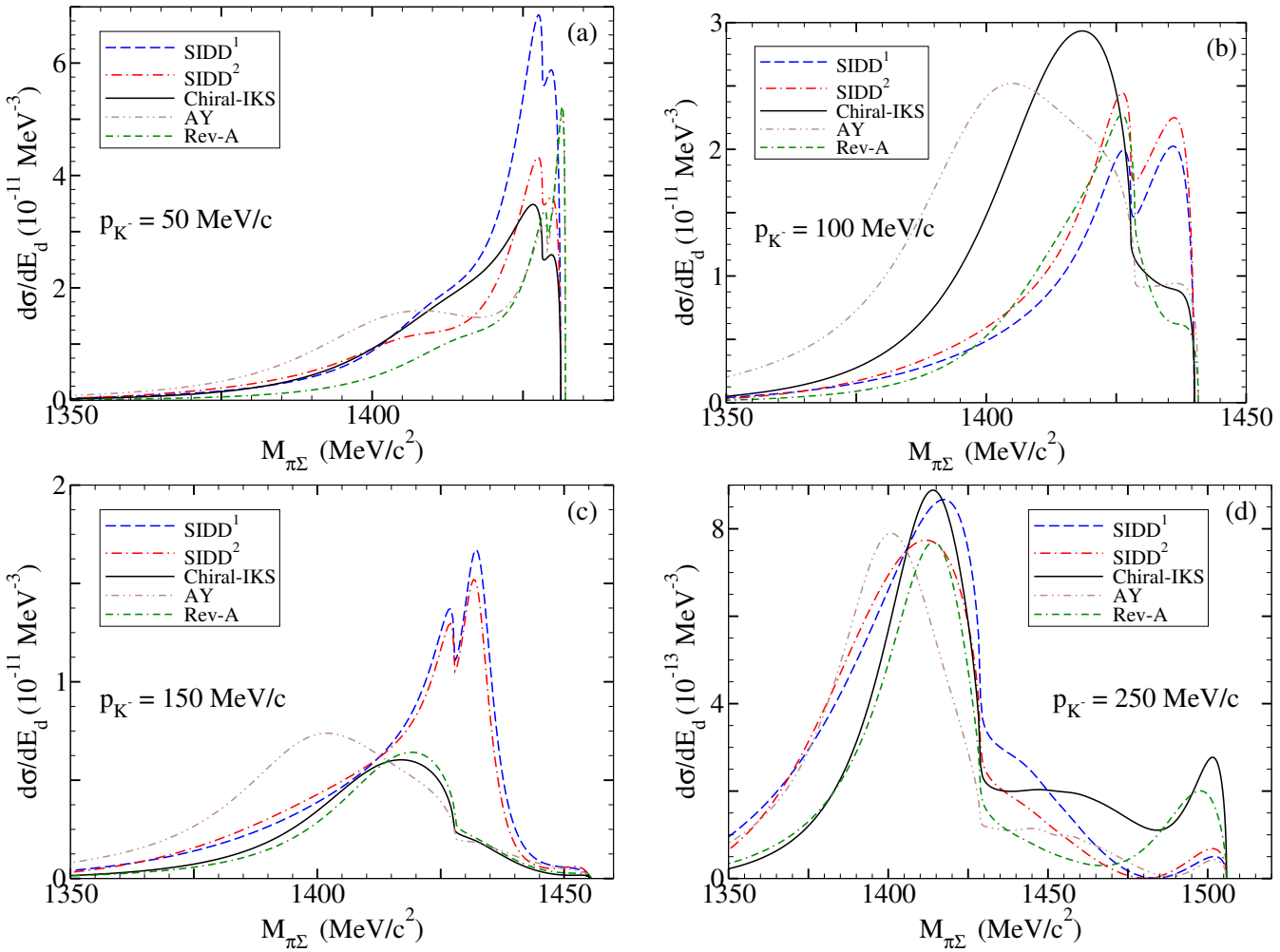

Fig. 3. (Color on line) The $\pi\Sigma$ mass spectra for $K^- + {}^3\mathrm{He} \to \pi^0\Sigma^0 + d$ reaction. Different types of $\bar{K}N - \pi\Sigma$ potentials were used. The kaon incident momentum is around $p_{\bar{K}}^{cm} = 50 - 250$ MeV/c. In panels (a), (b), (c) and (d), the values of $\bar{P}_K$ are 50, 100, 150 and 250 MeV/c, respectively. The blue dashed and red dash-dotted curves show the mass spectrum with SIDD^1 and SIDD^2 potential, respectively. The extracted results for Chiral-IKS, AY and Rev-A potentials are also depicted by black solid, brown dash-dot-dotted and green dash-dash-dotted lines, respectively.

Using Eq.(12), we define the break-up cross section of $\bar{K} + (Nd) \to d + (\pi^0\Sigma^0)$ as follows:

$$\frac{d\sigma}{dE_d} = \frac{\omega_{(Nd)}\omega_{\bar{K}}}{z\bar{p}_{\bar{K}}} \frac{m_\pi m_\Sigma m_d}{m_\pi + m_\Sigma + m_d} \int d\Omega_{p_d} d\Omega_{k_d} p_d k_d \times \sum_{if} |T_{(\pi\Sigma)+d \leftarrow \bar{K}+(Nd)}(\boldsymbol{k}_d, \boldsymbol{p}_d, \bar{p}_{\bar{K}}; z)|^2, \quad (13)$$

where E_d is the deuteron energy in the center-of-mass frame of $\pi\Sigma$, which is defined by

$$E_d = m_d + \frac{p_d^2}{2\eta_d}, \quad (14)$$

and the energies $\omega_{(Nd)}$ and $\omega_{\bar{K}}$ are the kinetic energy of $\bar{K}$ and Nd in the initial state.

Since the input energy of the AGS equations is above the $\bar{K}Nd$ threshold, the moving singularities will appear in the three-body amplitudes. To remove these standard singularities, we have followed the same procedure implemented in Refs. [59, 60]. Using the so called "point-method", we computed the cross section of $K^- + (Nd) \to \pi\Sigma + d$ reaction.

Starting from Faddeev AGS equations 5, the $\pi^0\Sigma^0$ invariant mass for $K^- + (Nd) \to \pi\Sigma + d$ reaction was calculated. In our calculation, we studied the dependence of the mass spectrum on the fundamental $\bar{K}N - \pi\Sigma$ interaction by using five different interaction models reproducing various pole structure for $\Lambda(1405)$ resonance. With this method, we extracted the $\pi\Sigma$ mass spectrum for different incident antikaon momentum $p_{\bar{K}}^{cm} = 50 - 250\mathrm{MeV}/c$. The extracted mass spectrum for momenta $p_{\bar{K}}^{cm} = 50 - 150\mathrm{MeV}/c$ is strongly affected by threshold effects, but for the momentum $p_{\bar{K}}^{cm} = 250\mathrm{MeV}/c$ the signature of the resonance is clearly visible. Furthermore, it was found that the $\pi\Sigma$ mass spectrum, reflecting the $\Lambda(1405)$ mass distribution and width, depends quite sensitively on the $\bar{K}N - \pi\Sigma$ model of interaction.

A definitive study of the three-body $\bar{K}Nd$ system could be also performed using the standard energy-dependent $\bar{K}N$ input potential, too [11]. The energy-dependent potentials provide a weaker $\bar{K}N$ attraction for lower energies than the energy-independent potentials. Therefore, the quasi-bound state in $\bar{K}N$ system resulting from the energy-dependent potential happens to be shallower. In Fig. 3, a comparison is made between the results obtained for the chiral-IKS $\bar{K}N - \pi\Sigma$ and the calculated mass spectra for other potentials. For energy-dependent potential the peak structure is not located at the position of the first pole given in table 1. These results are in agreement with the statement that the $\Lambda(1405)$ spectrum is the superposition of two independent states and one can not see two different pole structure in the $\Lambda(1405)$ spectrum [22,26].

The key point in the present calculations is the detection of deuteron which is a loosely bound system. Although, for large momenta the signal of $\Lambda(1405)$ overcomes the kinetic effects, at these energies, the probability for the deuteron (as a loosely bound system) to survive the reaction will decrease and one would expect a rather low reaction rate for $K^- + {}^3\mathrm{He} \to \pi\Sigma d$ reaction. Therefore, an accurate measurements of the $\pi\Sigma$ mass distribution at an optimized value of momentum in a possible future experiment could give a good reaction rate and less kinematical effects.

To study the dependence of the $\pi\Sigma$ invariant mass on the Nd model of interaction, in Fig. 4, we calculated the $\pi\Sigma$ mass spectra for two different Nd interaction, including a one-term (V_B^{Nd}) and a two-term (V_A^{Nd}) potential. Comparing the extracted invariant mass spectra for one-term potential and the corresponding mass spectra for the two-term potential, we can see that the Nd interaction can affect the mass spectra especially, for energies above the $\bar{K} + Nd$ mass threshold. However, the mass spectrum in energy region around the $\bar{K}N$ pole position did not change seriously by changing the Nd model of interaction.

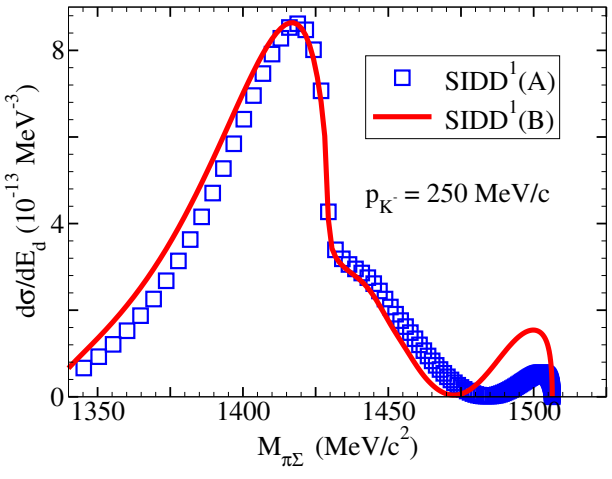

Fig. 4. (Color online) The invariant mass spectra for $K^- + {}^3\mathrm{He}$ reaction. We used the one-term (solid curves) and two-term (square symbols) potential for Nd interaction to study the dependence of the $\pi\Sigma$ mass spectra to the Nd model of interaction. The symbols A and B are corresponding to V_A^{Nd} and V_B^{Nd}, respectively. In our calculations, the one-pole version of SIDD potential was used to describe the $\bar{K}N$ interaction.

3.2 The coupled-channel AGS calculation of the $\bar{K}Nd - \pi\Sigma d$

In subsection 3.1, we solved the one-channel AGS equations for $\bar{K}Nd$ system and the decaying to the lower lying channels is included by using the so-called exact optical potential for $\bar{K}N$ interaction. In one-channel Faddeev calculations the effect of the $\tau_{\pi\Sigma\to\pi\Sigma}$ amplitude was excluded. Based on chiral unitary approach, the first and second pole of $\Lambda(1405)$ have clearly different coupling nature to the meson-baryon channels; the higher energy pole dominantly couples to the $\bar{K}N$ channel, while the lower energy pole strongly couples to the $\pi\Sigma$ channel. Due to the different coupling nature of these resonances, the shape of the $\Lambda(1405)$ spectrum can be different depending on the initial and final channels. In the $\bar{K}N \to \pi\Sigma$ amplitude, the initial $\bar{K}N$ channel gets more contribution from the higher pole with a larger weight. Consequently, the spectrum shape has a peak around 1420 MeV coming from the higher pole [22, 26]. This is obviously different from the $\pi\Sigma \to \pi\Sigma$ spectrum which is largely affected by the lower pole. Therefore, the extracted mass spectra in subsection 3.1 can not reproduce exactly the possible experimental mass spectra. To calculate the exact $\pi\Sigma$ mass spectra for $\bar{K} + (Nd)$ reaction, we solved the Faddeev equations for coupled-channel $\bar{K}Nd - \pi\Sigma d$ system. In addition to the above mentioned reaction, we need an interaction model for Σd and πd subsystems. In present calculations, the effect of πd interaction is neglected. To describe the Σd interaction, we used a one term complex potential in a form given in Eq. 11. To define the parameters of the Σd interaction, we used the Σd scattering length, which can be extracted from the Faddeev equations of the three-body $\Sigma(NN)_{s=1,I=0}$ system. The antisymmetric Faddeev equations for Σd system can be given by

$$\begin{aligned}
\mathcal{K}^{sI,s'I'}_{\Sigma,\Sigma} &= \sum_{s''I''} \mathcal{M}^{sI,s''I''}_{\Sigma,N_1}\, \tau^{s''I''}_{N_1}\, (\mathcal{K}^{s''I'',s'I'}_{N_1,\Sigma} - \mathcal{K}^{s''I'',s'I'}_{N_2,\Sigma}) \\
\mathcal{K}^{sI,s'I'}_{N_1,\Sigma} &- \mathcal{K}^{sI,s'I'}_{N_2,\Sigma} = 2\mathcal{M}^{sI,s'I'}_{N_1,\Sigma} \\
&+ \sum_{s''I''} 2\mathcal{M}^{sI,s''I''}_{N_1,\Sigma}\, \tau^{s''I''}_{\Sigma}\, \mathcal{K}^{s''I'',s'I'}_{\Sigma,\Sigma} \\
&- \sum_{s''I''} \mathcal{M}^{sI,s''I''}_{N_1,N_2}\, \tau^{s''I''}_{N_2}\, (\mathcal{K}^{s''I'',s'I'}_{N_1,\Sigma} - \mathcal{K}^{s''I'',s'I'}_{N_2,\Sigma})
\end{aligned} \tag{15}$$

where the Σd scattering length is given by

$$a_{\Sigma d} = -4\pi^2\, \mu_{\Sigma d}\, \mathcal{K}^{\frac{1}{2}1,\frac{1}{2}1}_{\Sigma,\Sigma}(p \to 0, p' \to 0; z = -E_d) \tag{16}$$

where $\mu_{\Sigma d}$ is the reduced mass of Σd and E_d is the binding energy of deuteron. To solve Eq. 15, we need as input a potential model for $\Sigma N - \Lambda N$ and NN interactions. In our three-body study, to describe the singlet and triplet ΣN interaction, we used the potentials given in Ref. [52] and for triplet NN interaction, we choose a potential of PEST type [61], which is a separablization of the Paris potential. The Σd scattering length value obtained with the two above mentioned $\Sigma N - \Lambda N$ and NN potentials is

$$a_{\Sigma d} = -1.59 + i0.71\ \mathrm{fm}^{-1} \tag{17}$$

The whole dynamics of coupled-channel $\bar{K}Nd$–$\pi\Sigma d$ three-body system is described in terms of the transition amplitudes $\mathcal{K}^{\alpha\beta;I_iI_j}_{i,m;j,n}$. The superscripts $\alpha,\beta=1,2$ are included to take into account the coupling between $\bar{K}Nd$ and $\pi\Sigma d$ systems. The Faddeev AGS equations for $\bar{K}Nd-\pi\Sigma d$ system can be expressed by

$$
\begin{aligned}
\mathcal{K}^{11;I_{\bar{K}}I_{\bar{K}}}_{\bar{K},m;\bar{K},n} &= \sum_{rr'}(\mathcal{M}^{1,I_{\bar{K}}I_N}_{\bar{K},m;N,r}\tau^{11;I_N}_{N(rr')}\mathcal{K}^{11;I_NI_{\bar{K}}}_{N,r';\bar{K},n} \\
&+ \mathcal{M}^{1,I_{\bar{K}}I_d}_{\bar{K},m;d,r}\tau^{11,I_d}_{d(rr')}\mathcal{K}^{11,I_dI_{\bar{K}}}_{d,r';\bar{K},n} + \mathcal{M}^{1,I_{\bar{K}}I_d}_{\bar{K},m;d,r}\tau^{12,I_d}_{d(rr')}\mathcal{K}^{21,I_dI_{\bar{K}}}_{d,r';\bar{K},n}) \\
\mathcal{K}^{11;I_NI_{\bar{K}}}_{N,m;\bar{K},n} &= \mathcal{M}^{1;I_NI_{\bar{K}}}_{N,m;\bar{K},n} + \sum_{rr'}(\mathcal{M}^{1;I_NI_{\bar{K}}}_{N,m;\bar{K},r}\tau^{11,I_{\bar{K}}}_{\bar{K}(rr')}\mathcal{K}^{11,I_{\bar{K}}I_{\bar{K}}}_{\bar{K},r';\bar{K},n} \\
&+ \mathcal{M}^{1,I_NI_d}_{N,m;d,r}\tau^{11,I_d}_{d(rr')}\mathcal{K}^{11,I_dI_{\bar{K}}}_{d,r';\bar{K},n} + \mathcal{M}^{1,I_NI_d}_{N,m;d,r}\tau^{12,I_d}_{d(rr')}\mathcal{K}^{21;I_dI_{\bar{K}}}_{d,r';\bar{K},n}) \\
\mathcal{K}^{11;I_dI_{\bar{K}}}_{d,m;\bar{K},n} &= \mathcal{M}^{1;I_dI_{\bar{K}}}_{d,m;\bar{K},n} + \sum_{rr'}(\mathcal{M}^{1;I_dI_{\bar{K}}}_{d,m;\bar{K},r}\tau^{11;I_{\bar{K}}}_{\bar{K}(rr')}\mathcal{K}^{11;I_{\bar{K}}I_{\bar{K}}}_{\bar{K},r';\bar{K},n} \\
&+ \mathcal{M}^{1;I_dI_N}_{d,m;N,r}\tau^{11;I_N}_{N(rr')}\mathcal{K}^{11;I_NI_{\bar{K}}}_{N,r';\bar{K},n}) \\
\mathcal{K}^{21;I_dI_{\bar{K}}}_{d,m;\bar{K},n} &= \sum_{rr'}\mathcal{M}^{2;I_dI_\pi}_{d,m;\pi,r}\tau^{22;I_\pi}_{\pi(rr')}\mathcal{K}^{21;I_\pi I_{\bar{K}}}_{\pi,r';\bar{K},n} \\
\mathcal{K}^{21;I_dI_{\bar{K}}}_{\pi,m;\bar{K},n} &= \sum_{rr'}(\mathcal{M}^{2;I_\pi I_d}_{\pi,m;d,r}\tau^{22;I_d}_{d(rr')}\mathcal{K}^{21;I_dI_{\bar{K}}}_{d,r';\bar{K},n} \\
&+ \mathcal{M}^{2;I_\pi I_d}_{\pi,m;d,r}\tau^{21;I_d}_{d(rr')}\mathcal{K}^{11;I_dI_{\bar{K}}}_{d,r';\bar{K},n}).
\end{aligned}
\tag{18}
$$

The break-up amplitude for $\bar{K}+(Nd)\to(\pi\Sigma)+d$ reaction in terms of the Faddeev transition amplitudes can be given by

$$
\begin{aligned}
&T_{(\pi\Sigma)+d\leftarrow(Nd)+\bar{K}}(\boldsymbol{k}_d,\boldsymbol{p}_d,\bar{P}_{\bar{K}};z) \\
&= \sum_n g^{I=0}_{\pi\Sigma}(\boldsymbol{k}_d)\tau^{I=0}_{\pi\Sigma\leftarrow\bar{K}N}(z-E_d(\boldsymbol{p}_d))\mathcal{K}^{11;;0\frac{1}{2}}_{d,1;\bar{K},n}(p_d,\bar{P}_{\bar{K}};z) \\
&+ \sum_n g^{I=0}_{\pi\Sigma}(\boldsymbol{k}_d)\tau^{I=0}_{\pi\Sigma\leftarrow\pi\Sigma}(z-E_N(\boldsymbol{p}_d))\mathcal{K}^{21;;0\frac{1}{2}}_{d,1;\bar{K},n}(p_d,\bar{P}_{\bar{K}};z) \\
&+ \sum_n \langle[\pi\otimes\Sigma]_{I=0}\otimes d \mid \pi\otimes[\Sigma\otimes d]_{I=1}\rangle g^{I=1}_{\Sigma d}(\boldsymbol{k}_\pi) \\
&\qquad\times\tau^{I=1}_{\Sigma d\leftarrow\Sigma d}(z-E_\pi(\boldsymbol{p}_\pi))\mathcal{K}^{21;1\frac{1}{2}}_{\pi,1;\bar{K},n}(p_\pi,\bar{P}_{\bar{K}};z),
\end{aligned}
\tag{19}
$$

where the momenta $\boldsymbol{p}_\pi$ and $\boldsymbol{k}_\pi$ are given by

$$
\begin{aligned}
\boldsymbol{p}_\pi &= \boldsymbol{k}_d - \frac{m_\pi}{m_\pi+m_\Sigma}\boldsymbol{p}_d \\
\boldsymbol{k}_\pi &= -\frac{m_d}{m_\Sigma+m_d}\boldsymbol{k}_d - \frac{m_\Sigma(m_\pi+m_\Sigma+m_d)}{(m_\pi+m_\Sigma)(m_\Sigma+m_d)}\boldsymbol{p}_d.
\end{aligned}
\tag{20}
$$

As one see from Eq. 19, in coupled-channel calculations plus the $\mathcal{K}^{11;;0\frac{1}{2}}_{d,1;\bar{K},n}$ amplitude, the effect of the $\mathcal{K}^{21;;0\frac{1}{2}}_{d,1;\bar{K},n}$ and $\mathcal{K}^{21;1\frac{1}{2}}_{\pi,1;\bar{K},n}$ are also included which accordingly, produces a more precise mass spectrum for $\pi\Sigma$. Inserting the new break-up amplitude (Eq. 19) in Eq. 13, we can calculate the $\pi\Sigma$ mass spectrum for $\bar{K}+(Nd)\to(\pi\Sigma)+d$ reaction. In Fig. 5, we calculated the $\pi\Sigma$ mass spectrum using different potential models for $\bar{K}N-\pi\Sigma$ interaction. As one can see from Fig. 5, in the fully coupled-channel calculations the resonance part of the mass spectrum is stronger and a more clear peak structure can be seen in $\pi\Sigma$ invariant mass. However, the observed peak structure of each model of $\bar{K}N-\pi\Sigma$ interaction is located at lower energies than those presented in Table 1, due to the momentum distribution in $p-d$ subsystem. By comparison of results using one-channel and coupled-channel Faddeev equations, it may be possible to study the effect of $\tau_{\pi\Sigma\to\pi\Sigma}$ amplitude on $\pi\Sigma$ invariant mass. As can be seen in Fig. 5, the extracted mass spectra in coupled-channel calculations are rather different from those by one-channel Faddeev calculations and it may be possible to discriminate between these two approaches. Therefore, the one-channel Faddeev calculations cannot be a strong tool to study the dynamics of $\Lambda(1405)$ resonance in $\bar{K}+(Nd)\to(\pi\Sigma)+d$ reaction.

As one can see in panel (B), an accurate measurements of the $\pi\Sigma$ mass distribution at $p_{K^-}=100\mathrm{MeV/c}$ can differentiate the AY and Rev-A potentials from the others and studying $K^-+{}^3\mathrm{He}$ reaction at $p_{K^-}=250\mathrm{MeV/c}$, one have a chance to discriminate between the other three potentials under the consideration. Looking at Fig. 5 one can clearly that for chiral energy-dependent potential, the magnitude of the mass spectrum above the $\bar{K}N$ threshold is considerably smaller than those by other potentials for all kaon incident momenta. Therefore, such a combined study at two different initial energies shows a big potential to discriminate between possible mechanisms of the formation of $\Lambda(1405)$ resonance.

4 Conclusion

In summary, the Faddeev-type calculations of $\bar{K}Nd$ system with quantum numbers $I=0$ and $s=\frac{1}{2}$ were performed. Solving the one-channel and full coupled-channel Faddeev equations for $\bar{K}Nd-\pi\Sigma d$ system, we calculated the $\pi\Sigma$ mass spectrum resulting from $K^-+{}^3\mathrm{He}\to\pi\Sigma d$ reaction by using the deuteron mass spectrum. The logarithmic singularities that appear when solving the AGS equations for the real scattering energies have been successfully handled by making use of the point method. To investigate the dependence of the resulting mass spectrum on models of $\bar{K}N-\pi\Sigma$ interaction, different phenomenological and chiral based potentials having the one- and two-pole structure of $\Lambda(1405)$ resonance, were used. We have examined how well the signature of the $\Lambda(1405)$ resonance manifests itself in the $\pi\Sigma$ invariant mass. By comparison of results using different interaction models, it was found that it may be possible to discriminate between different approaches describing the $\bar{K}N$ interaction.

The $\pi\Sigma$ mass spectrum was calculated for kaon incident momentum $p^{cm}_{K^-}=50-250$ MeV/c. However, the kinematical effects are important at low momenta and the signal of $\Lambda(1405)$ is masked, we have found that within our model for momenta above the 250 MeV/c, a clear bump produced by $\Lambda(1405)$ resonance appear in the $K^-+{}^3\mathrm{He}\to\pi\Sigma d$ cross section in the energy region between the $\bar{K}N$ and $\pi\Sigma$ thresholds, which strongly suggests that the clear signals of $\Lambda(1405)$ resonance should be detected by measuring of $\pi\Sigma$ invariant mass distributions at the relevant energies.

By performing the fully coupled-channel calculations for $\bar{K}Nd-\pi\Sigma d$ system, we studied the dependence of the $\pi\Sigma$ mass spectrum on the $\tau_{\pi\Sigma\to\pi\Sigma}$ amplitude. It was shown that

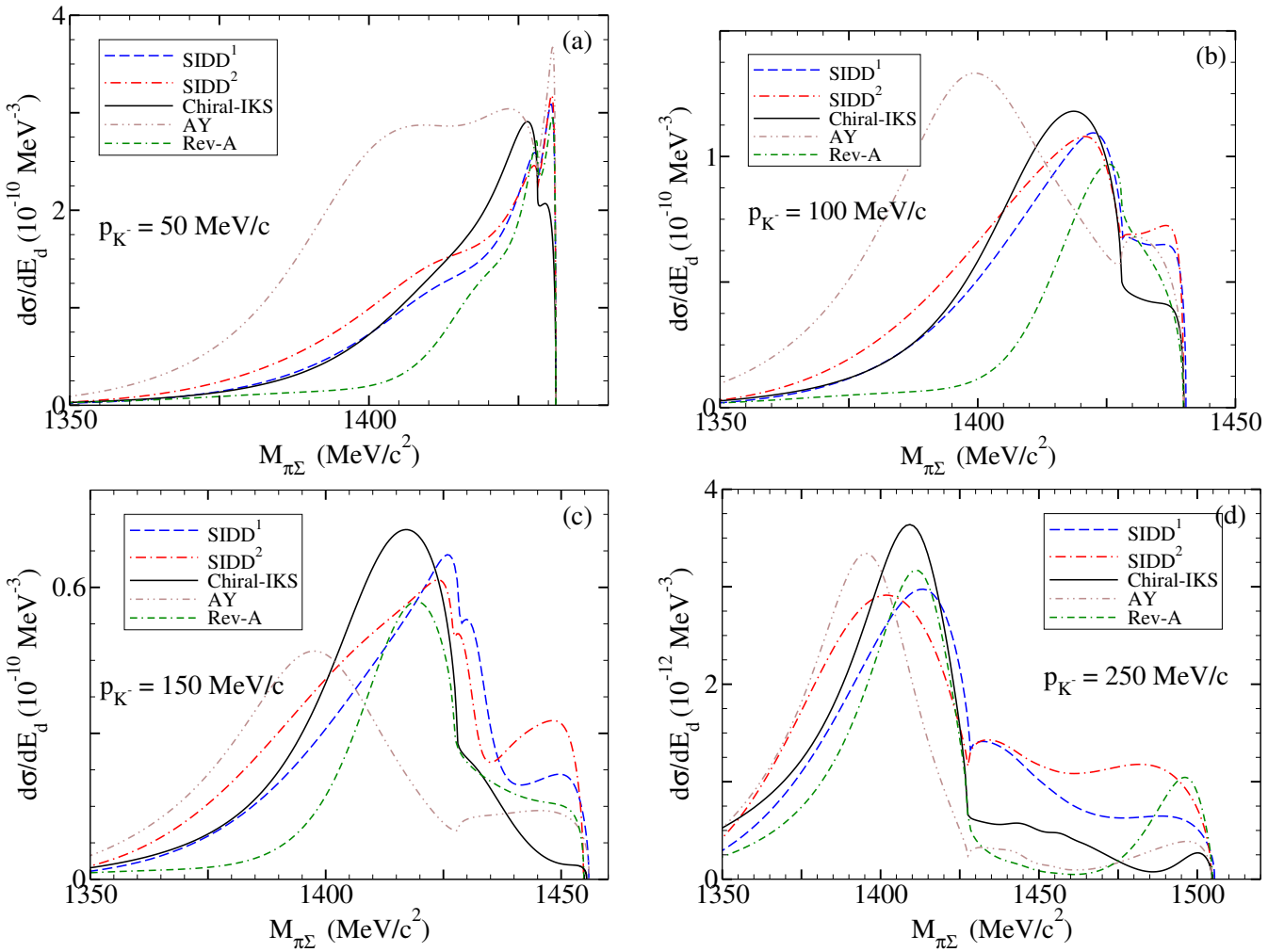

Fig. 5. (Color on line) Same as Fig.3, but in the present calculations, the full coupled-channel Faddeev AGS equations for $\bar{K}Nd - \pi\Sigma d$ system are solved.

the full coupled-channel calculations can produce a considerably different mass spectrum and the inclusion of the $\tau_{\pi\Sigma\to\pi\Sigma}$ amplitude is important for an exact study of the $\Lambda(1405)$ resonance structure.

This work has been financially supported by the research deputy of Shahrekord University. The grant number was 141/2843.

References

1. Y. Akaishi and T. Yamazaki, Phys. Rev. C **65**, 044005 (2002).
2. T. Yamazaki and Y. Akaishi, Phys. Lett. B **535**, 70 (2002).
3. A. Dote, H. Horiuchi, Y. Akaishi and T. Yamazaki, Phys. Lett. B **590**, 51 (2004).
4. A. Dote, H. Horiuchi, Y. Akaishi and T. Yamazaki, Phys. Rev. C **70**, 044313 (2004).
5. N. V. Shevchenko, A. Gal and J. Mares, Phys. Rev. Lett. **98**, 082301 (2007).
6. N. V. Shevchenko, A. Gal, J. Mares and J. Revai, Phys. Rev. C **76**, 044004 (2007).
7. Y. Ikeda and T. Sato, Phys. Rev. C **76**, 035203 (2007).
8. Y. Ikeda and T. Sato, Phys. Rev. C **79**, 035201 (2009).
9. A. Dote, T. Hyodo and W. Weise, Nucl. Phys. A **804**, 197 (2008).
10. A. Dote, T. Hyodo and W. Weise, Phys. Rev. C **79**, 014003 (2009).
11. Y. Ikeda, H. Kamano and T. Sato, Prog. Theor. Phys. **124**, 533-539 (2010).
12. S. Marri and S. Z. Kalantari, Eur. Phys. J. A **52**, 282 (2016).
13. S. Marri, S. Z. Kalantari and J. Esmaili, Eur. Phys. J. A **52**, 361 (2016).
14. S. Marri and J. Esmaili, Eur. Phys. J. A **55**:43 (2019).
15. S. Marri, S. Z. Kalantari and J. Esmaili, Chinese Physics C **43**, 064102 (2019).
16. S. Marri, Phys. Rev. C **102**, 015202 (2020).
17. R. H. Dalitz and S. F. Tuan, Phys. Rev. Lett. **2**, 425 (1959).
18. R. H. Dalitz and S. F. Tuan, Annals Phys. **10**, 307 (1960).
19. M. H. Alston, *et al.*, Phys. Rev. Lett. **6**, 698 (1961).
20. T. Yamazaki, Y. Akaishi, Phys. Rev. C **76**, 045201 (2007).
21. T. Hyodo and W. Weise, Phys. Rev. C **77**, 035204 (2008).
22. V. K. Magas, E. Oset, and A. Ramos, Phys. Rev. Lett. **95**, 052301 (2005).
23. D. Jido, J. A. Oller, E. Oset, A. Ramos and U. G. Meißner, Nucl. Phys. A **725**, 181 (2003).
24. B. Borasoy, R. Nißler and W. Weise, Eur. Phys. J. A **25**, 79 (2005).
25. B. Borasoy, U.-G. Meißner and R. Nißler, Phys. Rev. C **74**, 055201 (2006).
26. Z.-H. Guo and J. A. Oller, Phys. Rev. C **87**, 035202 (2013).

27. A. Feijoo, V. Magas, and A. Ramos, Phys. Rev. C **99**, 035211 (2019).
28. O. Braun, *et al.*, Nucl. Phys. B **129**, 1 (1977).
29. D. W. Thomas, A. Engler, H. E. Fisk and R. W. Kraemer, Nucl. Phys. B **56**, 15 (1973).
30. K. Moriya *et al.*, (CLAS Collaboration), Phys. Rev. C **87**, 035206 (2013).
31. K. Moriya *et al.*, (CLAS Collaboration), Phys. Rev. C **88**, 045201 (2013).
32. K. Moriya *et al.*, (CLAS Collaboration), Phys. Rev. Lett. **112**, 082004 (2014).
33. J. Ahn *et al.*, (LEPS Collaboration), Nucl. Phys. A **721**, 715 (2003).
34. M. Niiyama *et al.*, Phys. Rev. C **78**, 035202 (2008).
35. L. Roca and E. Oset, Phys. Rev. C **87**, 055201 (2013).
36. L. Roca and E. Oset, Phys. Rev. C **88**, 055206 (2013).
37. S. X. Nakamura and D. Jido, PTEP **2014**, 023D01 (2014).
38. M. Mai and U.-G. Meißner, Eur. Phys. J. A **51**, 30 (2015).
39. U.-G. Meißner and T. Hyodo, Chin. Phys. C **38**, 090001 (2014).
40. K. S. Myint, Y. Akaishi, M. Hassanvand and T. Yamazaki, arXiv:1804.08240v1 [nucl-ex].
41. G. Agakishiev *et al.*, (HADES Collaboration), Phys. Rev. C **87**, 025201 (2013).
42. H. Noumi *et al.*, (J-PARC proposal E31), http://j-parc.jp/researcher/Hadron/en/pac0907/pdf/Noumi.pdf (2009).
43. D. Jido, E. Oset, and T. Sekihara, Eur. Phys. J. A **42**, 257 (2009).
44. K. Miyagawa and J. Haidenbauer, Phys. Rev. C **85**, 065201 (2012).
45. D. Jido, E. Oset, and T. Sekihara, Eur. Phys. J. A **49**, 95 (2013).
46. J. Yamagata-Sekihara, T. Sekihara, and D. Jido, Prog. Theor. Exp. Phys. 2013, 043D02 (2013).
47. S. Ohnishi, Y. Ikeda, T. Hyodo, and W. Weise, Phys. Rev. C **93**, 025207 (2016).
48. K. Miyagawa, J. Haidenbauer and H. Kamada, Phys. Rev. C **97**, 055209 (2018).
49. J. Esmaili, Y. Akaishi and T. Yamazaki, Phys. Lett. B **686**, 23-28 (2010).
50. F. Sakuma *et al.*, (J-PARC E15 Collaboration), JPS Conf. Proc. **32**, 010088 (2020).
51. E. O. Alt, P. Grassberger, and W. Sandhas, Phys. Rev. C **1**, 85 (1970).
52. N. V. Shevchenko, Phys. Rev. C **85**, 034001 (2012).
53. N. V. Shevchenko, Nucl. Phys. A **890-891**, 50 (2012).
54. M. Bazzi *et al.*, (SIDDHARTA Collaboration), Phys. Lett. B **704**, 113 (2011).
55. J. Revai, Few-Body Syst. 61:32 (2020).
56. Y. Yamaguchi, Phys. Rev. **95**, 1628 (1954).
57. Z.-M Chen, W. Tornow and A. Kievsky, Few-Body Syst. **35**, 15-31 (2004).
58. N. V. Shevchenko and J. Revai, Phys. Rev. C **90**, 034003 (2014).
59. L. Schlessinger, Phys. Rev. **167**, 1411 (1968).
60. H. Kamada, Y. Koike, and W. Gloeckle, Prog. Theor. Phys. **109**, 869 (2003).
61. H. Zankel, W. Plessas, J. Haidenbauer, Phys. Rev. C **28**, 538 (1983).